Quasicritical Behavior of Dense-Gas Solvent-Solute Clusters at Near-Infinite Dilution

James A. O'Brien, Theodore W. Randolph, Claude Carlier, and Shankar Ganapathy
Dept. of Chemical Engineering, Yale University, New Haven, CT 06520

We compare molecular dynamics and electron paramagnetic resonance spectroscopic experiments on very dilute solutions of nitroxide free radicals in nearcritical and supercritical ethane. The measurement of the effective local density of solvent in the cybotactic region of the probe solute shows that maxima in local density enhancements occur in both computer and spectroscopic experiments at about half of the critical density, well removed from the maximum in the solvent's isothermal compressibility.

Remarkably, at the bulk density where the maximum enhancement occurs, we observed long-lived clusters in the vicinity of the solute molecule. Geometrically defined clusters persist for at least 100 picoseconds of simulated time. The persistence of these clusters is corroborated by the behavior of the solute diffusion coefficient, which shows fluctuating values over simulated time periods as long as 1.3 nanoseconds. We argue that fluctuations in the local solvent density about a solute molecule are not a long-ranged solvent critical effect. Rather, they represent a localized, short-ranged quasicritical phenomenon induced by the solute, which may be described in terms of a transition between weakly attractive and attractive behavior. We discuss the implications of time-varying microstructure for reactions in supercritical fluid media.

Introduction

Supercritical fluids offer many advantages as a milieu for reactions. Diffusivities are about an order of magnitude higher than those in liquids, and solubilities of solids can be much higher than those in gases at comparable temperatures. Perhaps most important is the fact that solvent properties (density, viscosity, dielectric, conductivity, and so on) can be varied over a wide range of values with relatively small changes in temperature or pressure. These varying solvent properties can in turn induce marked changes in reaction rate constants (Johnston and Haynes, 1987), in reaction equilibria (Peck et al., 1989), and even in reaction mechanisms (Ikushima et al., 1992). Yet, in spite of the numerous potential advantages of supercritical fluid solvents for reactions, understanding of supercritical fluid effects on reactions is still incomplete. A greater understanding of the fundamental physical chemistry of supercritical fluid mixtures is required to provide rational criteria to design supercritical fluid solvents for a particular reaction.

Correspondence concerning this article should be addressed to J. A. O'Brien or T. W. Randolph.

In particular, near-infinite dilution mixtures of supercritical fluids are interesting both for industrial application and theoretical reasons (Debenedetti, 1987). Indeed, as pointed out by Debenedetti and Chialvo (1992), most supercritical mixtures of practical interest are dilute in at least one component. In the case of a reacting system, it is imperative to understand the dilute-solution behavior (both dynamic and thermodynamic) of various components of the reaction mixture, such as catalysts and initiators.

The microstructure of supercritical fluid solvents has been implicated in several density-dependent solvent effects on reactions under supercritical conditions. Local, short-range structure in supercritical fluid mixtures may cause large deviations from bulk conditions in the local solvent density about a solute. Such local density augmentations have been observed in numerous spectroscopic studies (Brennecke and Eckert, 1988, 1989; Brennecke et al., 1990; Combes et al., 1992; Betts et al., 1992; Johnston et al., 1989; Kajimoto et al., 1988; Kim and Johnston, 1987; Yonker and Smith, 1988; Carlier and Randolph, 1993). In addition, local density augmentation of solutes

around solute molecules has been observed by EPR spectroscopy (Randolph et al., 1988) and by fluorescence spectroscopy (Brennecke et al., 1990), although the latter result appears to be in some doubt (Bright et al., 1991). According to existing theory (Kim and Johnston, 1987; Debenedetti, 1987), the local density enhancement ρ^{local}/ρ^{bulk} should exhibit a maximum near the maximum of the isothermal compressibility, which occurs at a reduced density near unity for temperatures near the critical temperature. In general, however, the experimental data on local solvent density enhancements reported in the literature either do not exhibit clear maxima or show maxima at lower reduced densities of about 0.2–0.6. Experimentally, the local density enhancement is far less sensitive to changes in temperature than is the isothermal compressibility. Kamlet and Taft π^* data plotted vs. Onsager reaction field for 2-nitroanisole in CO_2 at $T_r = 1.01$ and $T_r = 1.06$ are nearly indistinguishable (Yonker and Smith, 1988), and maxima in local density enhancements of ethane around di-*tert*-butylnitroxide differ only slightly between $T_r = 1.01$ and $T_r = 1.08$ (Carlier and Randolph, 1992). In contrast, the maximum in the isothermal compressibility of ethane varies by almost an order of magnitude between $T_r = 1.01$ and $T_r = 1.08$.

Computational approaches have also shed light on supercritical microstructure. Knutson et al. (1992) have shown that, at densities near 1/3 of the critical density and at slightly supercritical temperatures, solutions of Lennard-Jones molecules show significant short-range augmentation in solvent density in the vicinity of a solute. The local density enhancement ρ^{local}/ρ^{bulk} computed from molecular dynamics simulations was in qualitative agreement with estimates of enhancements from fluorescence spectroscopic measurements. The temperature dependence of the computed local density enhancements was weak, decreasing by less than a factor of two as temperature was increased from $T_r = 1.01$ to $T_r = 1.14$. Integral equation approaches have revealed long-range density correlations in the density of solvent molecules about a solute (Cochran et al., 1988; Cochran and Lee, 1990; McGuigan and Monson, 1990) resulting in large excess numbers of solvent molecules around a solute (for attractive mixtures). Indeed, Debenedetti (1987) has calculated solvent excesses of over 100 molecules based on partial molar volume data for naphthalene in CO_2. Excesses of over 100 solvent molecules were also calculated from integral equations using the Percus-Yevick closure for an attractive mixture of dilute Xe in Ne; negative excesses were seen for the repulsive mixture of dilute Ne in Xe (Wu et al., 1990). Similar results from molecular dynamics calculations showed that energetically defined solvent-solute clusters had a characteristic life span greater than 1.88 picoseconds (Petsche and Debenedetti, 1989).

Supercritical fluids are particularly interesting as candidates for free radical reactions. The high diffusivities exhibited in the supercritical state may serve to reduce cage effects, which in turn may reduce undesirable side reactions such as geminate pair recombination of free radical initiators (Odian, 1981). Supercritical carbon dioxide has recently been demonstrated to be a suitable solvent for free radical-based fluoropolymer synthesis, eliminating some of the need for ozone-depleting chlorofluorocarbons (DeSimone et al., 1992). We have been examining the effect of solvent structure on free radical reactions in supercritical ethane (Randolph and Carlier, 1992). Unusual behavior of reaction rate constants as a function of density led us to probe further the local solvent density around free radicals in ethane (Carlier and Randolph, 1993). To enhance our microscopic understanding of our own experimental results, we decided to undertake molecular simulations of a system chosen to mimic dilute solutions of the free radical di-*tert*-butylnitroxide (DTBN) in ethane. The methodology employed and the results obtained are described below.

Materials and Methods

Electron paramagnetic resonance spectroscopic measurement of local densities of ethane around DTBN molecules at near infinite dilution

The materials and methods for estimating effective local densities of ethane around the stable free radical DTBN have been described previously in greater detail (Carlier and Randolph, 1993; Randolph and Carlier, 1992). In short, nitrogen hyperfine coupling constants A_N for dilute (mole fraction about 10^{-5}) solutions of DTBN in near- and supercritical ethane were measured as a function of pressure and temperature. A_N values were fitted to experimental electron paramagnetic resonance (EPR) spectra using modified programs based on the EPR simulation programs of Schneider and Freed (1989). Effective local densities were computed on the basis of the solvatochromic theory of McRae (1956), using A_N values measured for seven nonhydrogen-bonding solvents as well as literature values (Knauer and Napier, 1976).

Simulations—general methods

Molecular dynamics and Monte Carlo simulations were carried out by approximating DTBN and ethane as spherical molecules, each characterized by Lennard-Jones (L-J) size and energy parameters σ and ϵ, that is, assuming the L-J potential functions:

$$\Gamma(r) = \begin{cases} 4\epsilon\left[\left(\frac{\sigma}{r}\right)^{12} - \left(\frac{\sigma}{r}\right)^{6}\right] & r < r_c \\ 0 & r \geq r_c \end{cases} \tag{1}$$

The minimum cutoff value, r_c, was $2.8\sigma_{12}$ which was equivalent to $3.69\sigma_{11}$ for our system. All quantities were made dimensionless in the usual way (Allen and Tildesley, 1986), using the properties of the solvent, component 1:

$T^* \equiv kT/\epsilon_{11}$	temperature
$\rho^* \equiv \rho\sigma_{11}^3$	density
$t^* \equiv t/(\sigma_{11}\sqrt{m_1/\epsilon_{11}})$	time
$r^* \equiv r/\sigma_{11}$	length
$D^* \equiv D\sqrt{m_1/\epsilon_{11}}/\sigma_{11}$	diffusivity

Infinite dilution was modeled using a single solute molecule in 599 solvent molecules, so each of our production simulations was for 600 molecules. While this corresponds to a mole fraction somewhat more than 0.001, the bulk solvent behavior seemed consistent with that of pure solvent (Appendix II). The L-J parameters and the methods by which they were chosen

are detailed below. All of our runs were at a dimensionless temperature $T^* = 1.42$, which corresponds to a reduced temperature of $T_r = 1.084$, using the best available value of $T_c = 1.31$ for the L-J fluid (Smit et al., 1989). A useful reference for those unfamiliar with the general techniques of molecular dynamics (MD), upon which we will not elaborate here, is the book by Allen and Tildesley (1986). We did make certain modifications to the usual MD techniques, particularly in the way of implementation, as detailed in Appendix I.

We carried out simulations over a range of densities, chosen to bracket the critical density of $\rho^* = 0.31$. For each density, all of the usual thermodynamic properties were computed such as the configurational internal energy and specific heat, the internal virial (and, therefore, the compressibility factor or the pressure), as well as microstructural information in the form of the radial distribution functions, $g_{11}(r)$ and $g_{12}(r)$. In addition, we computed the instantaneous sizes of clusters around both the lone solute molecule and one randomly-chosen solvent molecule. For these purposes, we defined a cluster in the geometric sense as the total excess number of solvent molecules within a certain distance of the molecule of interest. Two such distances were used, one corresponding approximately to a single shell of solvent molecules around a solute ($r = 1.87\sigma_{11}$) and the other to between two and three shells ($r = 3.0\sigma_{11}$).

Model parameters

While DTBN is actually dipolar, we have modeled both of our components using the nonpolar Lennard-Jones potential. Although the results of such a calculation are more qualitative than quantitative, previous workers have successfully justified this approximation, at least for the purposes of gaining preliminary insight into a problem (for example, Cochran and Lee, 1989).

L-J parameters for ethane ($\sigma = 5.22$ Å, $\epsilon = 0.812$ kcal/mol) were taken from Prausnitz (1969). A group contribution method was devised to estimate parameters for DTBN as follows. A multisite L-J model for DTBN was first constructed using the following groups: six methyl groups ($\sigma = 3.96$ Å, $\epsilon = 0.145$ kcal/mol) (Jorgensen et al., 1984); two tetrahedrally-bonded carbon atoms ($\sigma = 3.80$ Å, $\epsilon = 0.050$ kcal/mol) (Jorgensen et al., 1984); one nitrogen atom with trigonally planar bonds ($\sigma = 3.25$ Å, $\epsilon = 0.170$ kcal/mol) (Jorgensen et al., 1990); and an oxygen atom with either ketonal character ($\sigma = 2.96$ Å, $\epsilon = 0.210$ kcal/mol) (Jorgensen and Tirado-Rives, 1988) or hydroxyl character ($\sigma = 3.07$ Å, $\epsilon = 0.170$ kcal/mol) (Jorgensen, 1986). Based on structures of other nitroxide free radicals (Capiomont et al., 1972; Bordeaux et al., 1973; Lajzerowicz-Bonnetau, 1976), we used bond lengths and angles as follows: C-CH_3 bond lengths were taken as 1.52 Å, the N-O bond length as 1.26 Å, and the C-N bond lengths as 1.482 Å. CH_3-C-CH_3 bond angles were assumed to be 109.47°, and the three planar bond angles to the nitrogen were assumed to be 120°.

The average potential Γ_{12} between a DTBN molecule and an ethane molecule, at a given separation distance r between their two respective centers of mass, was calculated by averaging the sum of L-J contributions from all nine groups over all solid angles. The separation was varied in 0.1 Å increments and both polar angles in 5° increments, to construct a spherically averaged $\Gamma_{12}(r)$ curve; the average was weighted by the size of each volume element. Since DTBN is very nearly spherical, little angular dependency of the potential was observed, except at very small separations. The unlike-pair L-J parameters σ_{12} and ϵ_{12} were then estimated by fitting the L-J potential to the $\Gamma_{12}(r)$ curve. Finally, pure component L-J parameters σ_{22} and ϵ_{22} for DTBN were calculated using a geometric combining rule for both σ and ϵ. While this differs from the more typical arithmetic averaging for σ, it is consistent with the approach of Jorgensen and coworkers (1984, 1986, 1988, 1990) upon whose group L-J parameters our potential is based. Two sets of L-J parameters for DTBN were calculated, attributing either a) a ketonal or b) a hydroxyl character to the oxygen of DTBN; the results differed only slightly, so an average of the two was used in all subsequent calculations. The final values of the L-J parameters used in all simulations are shown in Table 1.

Table 1. Lennard-Jones Parameters Used in Simulations

	σ_{ij} [Å]	ϵ_{ij} [kcal/mol]
ethane-ethane	5.22	0.386
ethane-DTBN	6.89	0.578
DTBN-DTBN	9.09	0.865

We are not aware of any thermodynamic data that would permit an assessment of the quality of the L-J parameters we have estimated for DTBN. Therefore, to check the estimates of L-J parameters we compared the critical properties of DTBN as calculated from group contribution methods to those resulting from our L-J parameters. Critical temperatures for DTBN calculated by the methods of Ambrose, Joback and Fedors (Reid et al., 1977) ranged from 545 K to 608 K, depending on the method and on the character (ketonal or hydroxyl) of the oxygen atom. The critical temperature of DTBN calculated from the L-J parameters (using $T_{cij} \equiv 1.31\epsilon_{ij}/k$) is 570 K, in good agreement with critical temperature estimates from other group contribution methods. For comparison, the L-J parameters for ethane give a critical temperature of 262 K, while the actual value is 305.4 K. Another check of the L-J parameters shows that the ratio σ_{22}/σ_{11} is close to the cube root of the ratio of molecular masses (1.73 vs. 1.69).

Local density enhancements from MD simulations

Following the example of Knutson et al. (1992), we compute the local density enhancement $\rho^{\text{local}}(r)/\rho^{\text{bulk}}$ from the modified partial fluctuation integral G'_{12}:

$$\frac{\rho^{\text{local}}}{\rho^{\text{bulk}}}(r) = 1 + \frac{3G'_{12}(r)}{\rho^{\text{bulk}} 4\pi(r^3 - r_{\min}^3)} \tag{2}$$

where

$$G'_{12}(r) \equiv 4\pi\rho^{\text{bulk}} \int_{r_{\min}}^{r} r^2[g_{12}(r) - 1]dr \tag{3}$$

and $r_{\min}$ is the separation at which g_{12}, the radial distribution function, first becomes significantly nonzero (here nearly constant at $r = 1.19\sigma_{11}$). Local density enhancements were computed for two radial values, $r = 1.87\sigma_{11}$ and $r = 3.0\sigma_{11}$.

Results

Computed local density enhancements are shown in Figure

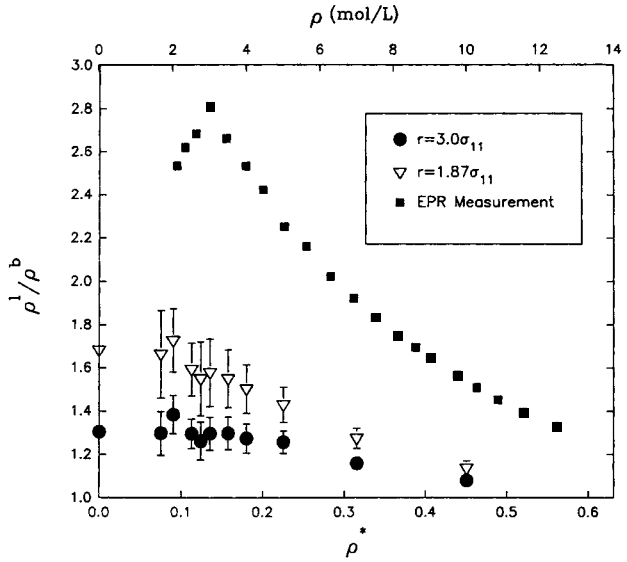

Figure 1. Dimensionless density enhancement against both dimensionless density ρ^* and corresponding density ρ.

●, ▽ = MD results for two different radial positions; ■ = EPR spectroscopic measurements (Carlier and Randolph, 1992). Analytic zero-density results on the two lower (MD) curves, ρ^{local}/ρ^{bulk}, computed in this manner (Eq. 2) are not unity at low density. Error bars represent 95% confidence intervals.

1. Each point is the result of a 200,000-step MD run, representing a real time span of 1,350 ps. The results from EPR spectroscopic experiments, nominally taken at the same reduced temperature ($T_r = 1.08$), are also shown in the same plot. It should be noted that local density effects on the nitrogen hyperfine coupling constant fall off with an r^{-6} radial dependence; thus, the EPR experiment probes at most two solvent shells. While the gross features are similar, the most striking difference is that the experimental local density enhancement

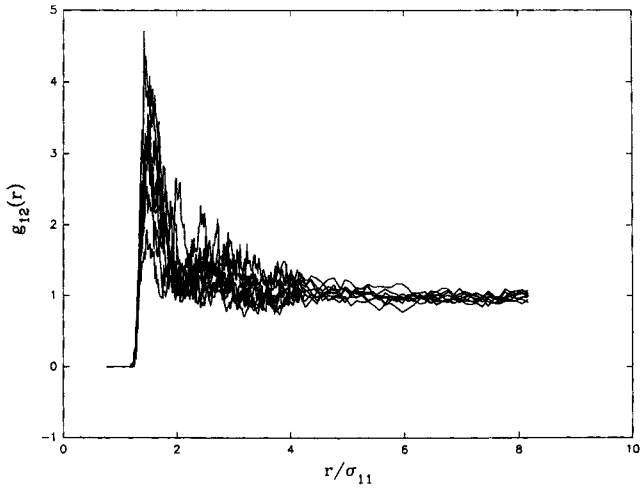

Figure 2. Radial distribution functions, subaveraged over long production simulations.

Each curve in this figure corresponds to an average over 10,000 MD steps during the course of a 200,000-step simulation at $\rho = 3.0$ mol/L. There are obviously large fluctuations over the course of the simulation.

is always larger than the enhancement computed by simulations, and the disagreement between experiment and computation reaches a maximum at about one-third to one-half the critical density ($\rho^* = 0.31$). A maximum in the experimental results is clearly seen, while the computed results show a muted maximum at best. This subdued maximum is in good agreement with the computations of Knutson et al. (1992), who showed a maximum in local density enhancement for the pyrene-CO_2 system that was clearly evident at $T_r = 1.02$ and grew progressively weaker as temperature was increased.

To estimate the computational uncertainty in the local density measurements, we calculated local density enhancements every 10,000 MD steps (67 ps) over the duration of a 200,000-step MD run. (Data recording was always preceded by a 4,000-step melt-and-anneal equilibration sequence.) Error bars for the local density enhancements plotted in Figure 1 are 95% confidence limits based on these 20 measurements. It is interesting to note that the error bars are the largest at about one-half the critical density, rather than at the critical density, where long-ranged solvent fluctuations might be expected to cause greater variability, or at the lowest densities, where statistics are poor. In fact, the error bars are surprisingly large; 67 ps is apparently not a period of sufficient duration to accurately probe the thermodynamic average local density. For a given measurement taken over 67 ps, the 95% confidence limits would be $\sqrt{19}$ larger, so that the upper error bars would very nearly match the spectroscopically-measured local density enhancements. As will be discussed later, this may not be mere coincidence. X-band EPR spectroscopy operates at a frequency of about 10 GHz or a characteristic time period of about 100 ps. Thus, processes with a duration of order 100 ps will strongly affect the EPR results and give rise to large uncertainties in computations carried out over similar time spans.

It is instructive then to examine the uncertainty in the computational results in greater detail. Figure 2 shows a plot of $g_{12}(r)$ vs. radial separation distance at a density of $\rho^* = 0.131$ for 20 consecutive runs of 10,000 MD steps (67 ps) each. Over the time span of the entire simulation (>1 ns) there are very large variations in $g_{12}(r)$, especially at small separations. As shown in Figure 3, such temporal variations are even more apparent in plots of $G_{12}(r)$, the excess number of solvent molecules around the solute:

$$G_{12}(r) \equiv 4\pi\rho^{bulk}\int_0^r r^2[g_{12}(r) - 1]dr, \qquad (4)$$

These results are again plotted every 10,000 MD steps over the course of a 200,000-step MD simulation, but this time for a system of three times the size (1 solute molecule in 1,799 solvent molecules). It is evident that the number of excess solvent molecules around the solute undergoes fluctuations which persist for at least 10,000 MD steps. The dark line is the prediction of integral equation theory in the Percus-Yevick approximation (McGuigan and Monson, 1990); it appears to represent well the mean simulation result.

The density dependence of the fluctuations in local solvent density is also remarkable. Figure 4a shows the standard deviation of the excess number of solvent molecules around a solute as a function of bulk density for two different radial separations. The standard deviation is calculated from 20 con-

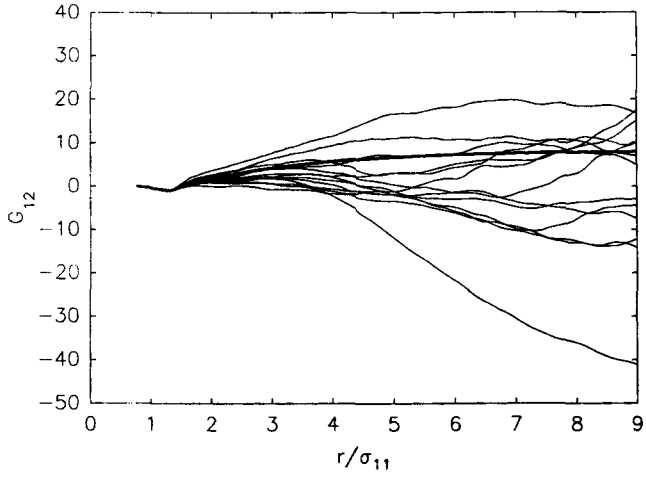

Figure 3. Partial fluctuation integrals against distance, subaveraged over long production simulations.

Each curve corresponds to an average over 10,000 MD steps during the course of a 200,000-step simulation at $\rho = 3.0$ mol/L. Results were obtained using a tripled system containing 1 solute molecule in 1,799 solvent molecules. The thick line is the corresponding result computed using integral equation theory in the Percus-Yevick approximation.

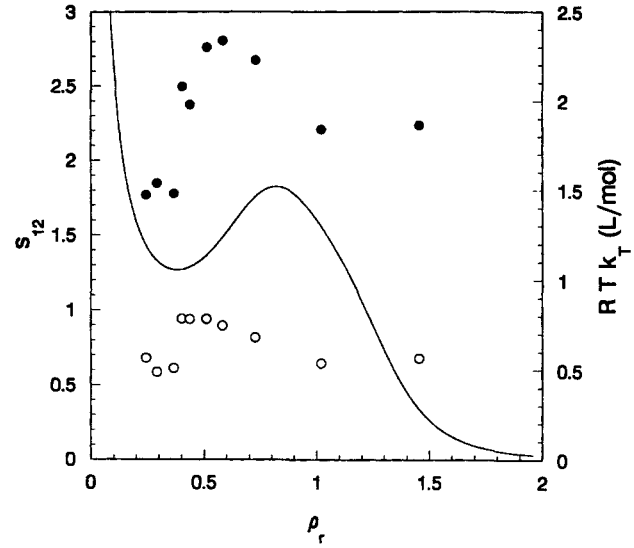

Figure 4a. Cluster fluctuations against density.

s_{12} is the standard deviation of the instantaneous solvent cluster size around a solute molecule, observed over 67 ps (10,000 MD steps). The peak at a reduced density ρ_r of about 0.5 indicates larger relative fluctuations of these clusters in this density regime. ● = molecules within a radius $r = 3\sigma_{11}$; ○ = those within $r = 1.87\sigma_{11}$. The line is the isothermal compressibility of the solvent (computed from the L-J equation of state) which peaks close to the critical density.

secutive MD runs, each of 10,000 MD-step duration. A strong maximum is seen at a reduced density near $\rho_r = 0.5$, indicating larger relative fluctuations in local solvent density in this density regime. For comparison, the isothermal compressibility of the solvent, computed using the L-J equation of state of Nicolas et al. (1979) is also plotted in Figure 4a. The maximum in isothermal compressibility, where critical clustering effects are expected to be most pronounced, occurs close to the critical density, rather than at 0.5.

In contrast, as shown in Figure 4b, the standard deviation of the excess number of solvent molecules around a randomly-chosen solvent molecule is about an order of magnitude smaller and tends to peak closer to the maximum in isothermal compressibility. In this system of limited size, solvent-solute clustering effects cause "echoes" in solvent-solvent interactions, so it is difficult to separate the two. This is because the particular solvent molecule around which we are counting other solvent molecules may, during the course of the simulation, become part of the cluster surrounding the solute, which in turn has a long persistence. However, it is apparent that the solvent-solute density fluctuations are much more pronounced than any fluctuations in solvent-solvent density, at least at this temperature. (Closer to the solvent's critical temperature, it is expected that solvent-solvent clusters would be the most pronounced.)

While the standard deviation of the excess number of solvent molecules around a solute provides useful information, little temporal information can be obtained, except to note that the process causing the high standard deviation must persist for times of the same order of magnitude as the observation period (10,000 MD steps, 67 ps). To further probe the time dependency of solvent-solute density fluctuations, we recorded the instantaneous number of solvent molecules in a shell of thickness $1.87\sigma_{11}$ or $3.0\sigma_{11}$ surrounding the solute molecule every 0.2 ps for a run of total time of 1.3 ns. We then subtracted the mean number of solvent molecules around the solute to obtain an instantaneous excess number. These instantaneous excesses were autocorrelated in time by Fourier transform techniques, using the commercial signal processing software package DADiSP. Figure 5 shows the autocorrelation functions for the number of solvent molecules around a solute, and for solvent molecules around a randomly-chosen solvent, both as a func-

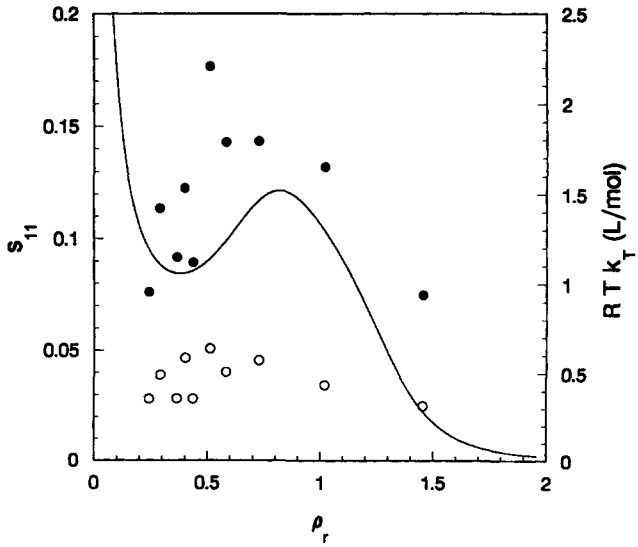

Figure 4b. Cluster fluctuations against density.

s_{11} is the standard deviation of the solvent cluster size around a solvent molecule, observed over 67 ps (10,000 MD steps). The key is the same as for Figure 4a; the peak in s is now much smaller and occurs nearer the critical density.

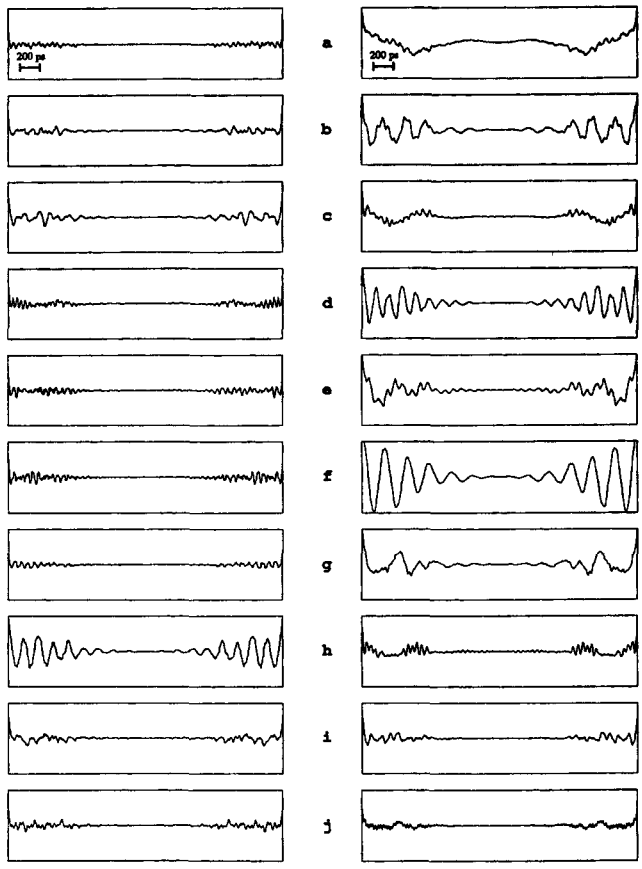

Figure 5. Autocorrelation functions of instantaneous solvent-solvent and solute-solvent clusters.

Solvent-solvent ACFs are on the left panel and solvent-solute ACFs on the right. Each horizontal pair corresponds to a particular ethane density in [mol/L]: $a = 1.67$, $b = 2.0$, $c = 2.5$, $d = 2.75$, $e = 3.0$, $f = 3.5$, $g = 4.0$, $h = 5.0$, $i = 7.0$, and $j = 10.0$. Plotted functions were obtained by taking the time autocorrelation of (instantaneous cluster size at $r = 3.0\sigma_{11}$ less its mean, normalized by its standard deviation) and then autocorrelating a second time. There are dramatic effects, but the solute-solvent effect occurs at about half of the critical density (panels *d–f*) while the solvent-solvent effect occurs at the maximum in the isothermal compressibility (*h*). Abscissa in each case represents 2.7 ns, a time equal to twice the total simulation time. There are pronounced phenomena which occur only several times per simulation run.

tion of bulk density. The abscissa in each case represents a time equal to twice the run time (2.7 ns). Strong periodicity is seen in the autocorrelation function of the solvent-solute fluctuations, especially in the reduced density region of about 0.4–0.5. In this region, the most pronounced fluctuations have a remarkably long lifetime of about 200 ps.

In sharp contrast, there is very little structure evident in the autocorrelation function of the solvent fluctuations about a randomly-chosen solvent molecule. A notable exception occurs near the solvent's critical density, where well-defined periodicity is apparent. These results indicate that the solvent-solvent clusters have longer persistence at the critical density of the solvent, whereas the solute-solvent clusters become persistent at a lower density.

The ultimate goal of this work is to enhance our understanding of reaction processes in supercritical fluid media. Since it is likely that the rates of very fast reactions such as spin-exchange are transport-limited (Randolph and Carlier,

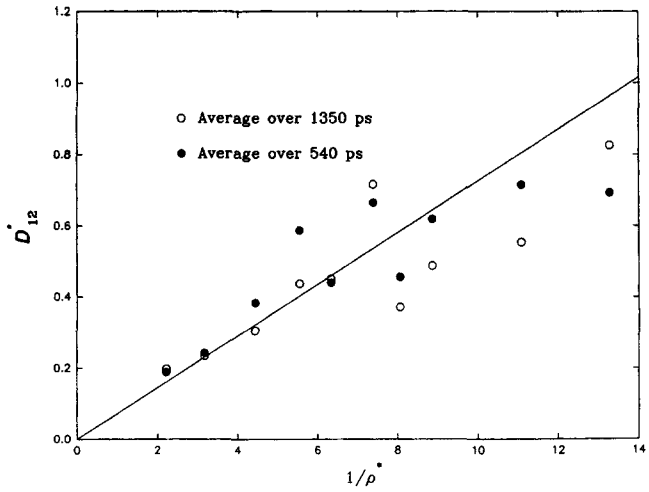

Figure 6a. Diffusion coefficient of solute, D^*_{12}, against reciprocal reduced density, $1/\rho^*$.

Straight line through the points is the best-fit line from Figure 6b, scaled by the ratio of diffusion coefficients predicted by Chapman-Enskog theory (Appendix II).

1993), we determined the diffusion coefficient of the lone solute in the solvent, D^*_{12}, and the self-diffusion coefficient of the solvent, D^*_{11}, in each of our simulations. The diffusion results provide further evidence for the existence of the temporal density correlations described above. Figures 6a and 6b are plots of D^*_{12} and D^*_{11}, respectively, against $1/\rho^*$. Note the large scatter in Figure 6a, at intermediate values of the dimensionless density, ρ^*. It becomes more difficult to obtain a good estimate of D^*_{12} at precisely the same range of densities where the long-lived clusters, described above, are present. This is reasonable since, if the cluster surrounding the solute is sufficiently persistent, the solute will spend much of the simulation period diffusing in an anomalous environment. The straight line in Figure 6a was computed from the best-fit line on Figure 6b, dividing the slope by 2.7, the ratio of D^*_{11}/D^*_{12} given by Chapman-Enskog theory (Reid et al., 1977; see also Appendix II).

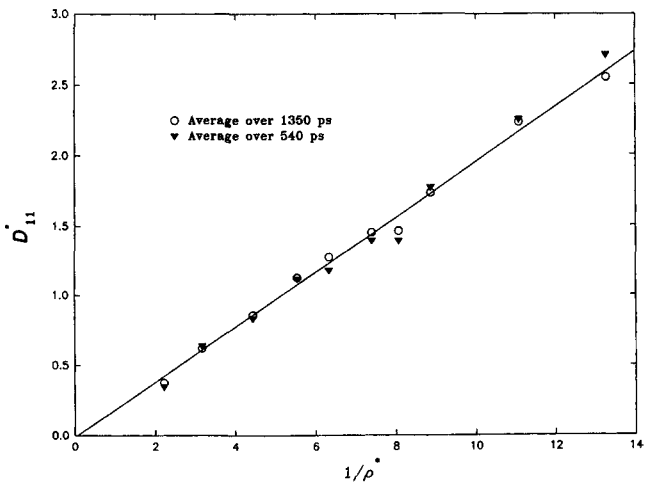

Figure 6b. Diffusion coefficient of solvent, D^*_{11}, against reciprocal reduced density, $1/\rho^*$.

The straight line through the points is a least-squares fit to all points.

For D_{11}^*, on the other hand, no such effect is evident, and the self-diffusion coefficient of the solvent varies roughly linearly with $1/\rho^*$, as required by Chapman-Enskog theory (Reid et al., 1977). The straight line through the points is a least-squares best fit to all of the plotted points. Since the self-diffusion coefficient was determined using ten times as many molecules as for D_{12}^* (see Appendix I), it might be fairer to scale the scatter in Figure 6a by a factor of $3(=\sqrt{10-1})$. Even in this case, however, the discrepancies are clearly evident.

Discussion

The density of solvent around solute molecules fluctuates dramatically within the first few solvent shells; these fluctuations have remarkably long periods. Because we are operating close to the solvent's critical temperature, it is tempting to propose that the effect is related to the critical behavior of the solvent. However, closer examination reveals that the effect does not scale with the isothermal compressibility of the solvent and, therefore, is not likely to be associated with long-ranged solvent critical fluctuations. Indeed, the most dramatic solvent-solute density fluctuations are seen at a density of about one-half of the solvent's critical density and are much less sensitive to temperature than is the isothermal compressibility of the solvent.

These observations suggest that a solute induces local behavior in the solvent that is reminiscent of critical behavior in the pure solvent. This behavior, however, is different from pure-fluid critical behavior in at least one important aspect: it is a short-ranged molecular effect. This short range guarantees that the effect has limited influence on bulk solvent thermophysical properties. Despite the absence of bulk effects, short-ranged phenomena having characteristic times comparable to the cluster fluctuation period, such as chemical reactions, may still be affected when the reaction rate depends strongly on microtransport behavior (such as cage effects). This is evident from the temporal variation of solute diffusivities measured over such time scales.

This viewpoint is supported by the classification scheme of Debenedetti and coworkers (Debenedetti and Mohamed, 1989; Petsche and Debenedetti, 1991) for solute-solvent interactions in nearcritical fluids. In this scheme, systems are classified as repulsive, weakly attractive, or attractive, based on whether the infinite-dilution direct correlation function integral C_{12}^∞ is less than 0, between 0 and 1, or greater than 1, respectively. In the limit where solute and solvent become identical, the boundary between weakly attractive and attractive behavior at $C_{12}^\infty = 1$ corresponds to the pure fluid critical point or $C_{11}^\infty = 1$. In mixtures, the boundary implies a change in sign of the partial molar volume of the solute, $\bar{V}_2^\infty$, from positive (solubility depression) under weakly attractive conditions, to negative (solubility enhancement) under attractive conditions.

The density at which C_{12}^∞ becomes unity may be computed for a van der Waals fluid (Petsche and Debenedetti, 1991) using:

$$T_r = \frac{3\rho_r \alpha^{1/2}(3-\rho_r)^2}{4[3+\rho_r(\gamma-1)]} \tag{5}$$

where $\alpha \equiv a_2/a_1$, the ratio of van der Waals a parameters for solute and solvent, respectively, and $\gamma \equiv b_2/b_1$, the corresponding b parameter ratio. Through corresponding states theory,

$$\alpha = \left(\frac{\sigma_2}{\sigma_1}\right)^3 \left(\frac{\epsilon_2}{\epsilon_1}\right) \tag{6a}$$

$$\gamma = \left(\frac{\sigma_2}{\sigma_1}\right)^3 \tag{6b}$$

Using the L-J parameters in Table 1, we compute using Eq. 5 a weakly attractive/attractive transition at $T_r = 1.08$ ($T^* = 1.42$) and $\rho_r = 0.21$. In contrast, both EPR and MD measurements show the maximum effect at $\rho_r = 0.45$. While the agreement is only approximate, it is interesting to note that exactly the same discrepancy was observed by Knutson et al. (1992) for the pyrene-CO_2 system; for the latter system, we compute a weakly attractive/attractive boundary at $T_r = 1.01$ and $\rho_r = 0.14$, whereas the local density enhancements from MD calculations showed a maximum at about $\rho_r = 0.33$. It is likely, therefore, that the discrepancy in both cases is due entirely to the inadequacy of the approximate model on which the boundary computation is based and that the actual weakly attractive/attractive boundary is closer to the value measured in both sets of MD simulations. Further, the boundary is relatively insensitive to temperature in the region of interest. For the DTBN-ethane system, the boundary shifts from $\rho_r = 0.21$ at $T_r = 1.08$ to $\rho_r = 0.19$ at $T_r = 1.01$. In a similar fashion, maxima in local density enhancements measured by EPR (Carlier and Randolph, 1992) shift only slightly on going from $T_r = 1.01$ to $T_r = 1.08$.

Therefore, we conjecture that the local behavior observed in the simulations and in the EPR measurements is a manifestation of *local quasicriticality* about an infinitely dilute solute molecule. The behavior occurs at bulk conditions corresponding to the weakly attractive/attractive boundary; for a pure fluid, this is precisely the critical point. In dilute mixtures, critical behavior at the weakly attractive/attractive boundary is limited to the immediate vicinity of a solute molecule. At these conditions, a small positive perturbation in local solvent density around a solute molecule causes the system to become more attractive, whereas a negative perturbation causes it to become more repulsive in nature. These effects are obviously cooperative, and on the local level the boundary is an unstable condition. This instability, coupled with material balance requirements, may well be at the root of the persistent clusters we have observed in our MD simulations.

Conclusions

We have demonstrated, using both MD simulation and EPR spectroscopy, a long-lived clustering phenomenon of solvent around solutes at infinite dilution in solvent fluids near their critical temperature. We conjecture that this is due to a phenomenon we have termed local quasicriticality. Geometrically defined clusters, which exhibit lifetimes of order 100 ps, are observed at densities near the weakly attractive/attractive boundary. Such long-lived clusters may in turn influence: microtransport properties, as shown by molecular dynamics diffusivity measurements; local density enhancement measurements, as shown by EPR spectroscopy; and even reaction rate constants (Randolph and Carlier, 1992). These clusters are short-ranged in nature and not strongly correlated with the isothermal compressibility of the solvent.

As shown by the comparison of the MD and EPR results,

care must be taken in relating spectroscopic results to thermodynamic properties. The persistence of the clusters, combined with the intrinsic nonlinearity of the spectroscopy's response to local density, may sometimes lead to results that say more about kinetics than they do about thermodynamics. Difficulties in relating spectra to thermodynamic properties will be most pronounced under conditions where quasicritical clusters have life spans of the same order of magnitude as the characteristic period of the spectroscopic technique. In fact, we see maximum discrepancy between EPR and MD measurements of local density enhancements in the density regime where the 100 ps life span of the clusters corresponds to the 10 GHz frequency of the stimulating microwave radiation of X-band EPR spectroscopy.

Acknowledgment

Acknowledgment is made to the donors of the Petroleum Research Fund, administered by the American Chemical Society, for partial support of this work (TWR). Further acknowledgment is made to the National Science Foundation for their support (through Grant BCS-9014119 and a Presidential Young Investigator Award to TWR, and Grant CBT-8809548 to JO'B). The authors thank Professor Peter A. Monson for the computer program used for the Percus-Yevick calculations and Professor Keith E. Gubbins for a preprint of the paper by Johnson et al. (1992).

Notation

Acronyms and abbreviations

ACF = autocorrelation function
DTBN = the free radical di-*tert*-butylnitroxide
EPR = electron paramagnetic resonance
L-J = Lennard-Jones
MC = Monte Carlo
MD = molecular dynamics
NVE = conditions of constant number of molecules, volume and internal energy (microcanonical ensemble)
NVT = conditions of constant number of molecules, volume and temperature (canonical ensemble)

Greek letters

α = ratio of van der Waals constants (Eq. 5)
γ = ratio of van der Waals constants (Eq. 5)
$\Gamma(r)$ = Lennard-Jones potential energy function
ϵ = L-J well-depth energy parameter
κ_T = isothermal compressibility
ρ = molar density
σ = L-J molecular diameter size parameter

Subscripts

11,1 = property of solvent, component 1
22,2 = property of solute, component 2
12 = solvent-solute cross property
c = critical property
r = reduced property

Superscripts

bulk = property of the bulk solvent
local = property of the solvent close to the solute
* = dimensionless property/parameter

Literature Cited

Allen, M. P., and D. J. Tildesley, *Computer Simulation of Liquids*, Oxford University Press, New York (1987).

Betts, T. A., J. Zagrobelny, and F. V. Bright, "Elucidation of Solute-Fluid Interactions in Supercritical CF_3H by Steady-State and Time-Resolved Fluorescence Spectroscopy," *Supercritical Fluid Technology*, F. V. Bright and M. E. P. McNally, eds., *ACS Symp. Ser.*, **448**, 48 (1992).

Bordeaux, D., J. Lajzerowicz, R. Briere, H. Lemaire, and A. Rassat, "Détermination des Axes Propres et des Valeurs Principales du Tensor *g* dans Deux Radicaux Libres Nitroxydes par Etude de Monocristaux," *Organic Magnetic Resonance*, Vol. 5, 47, Heyden & Son (1973).

Brennecke, J. F., and C. A. Eckert, "Fluorescence Spectroscopy Studies of Intermolecular Interactions in Supercritical Fluids," *Supercritical Fluid Science and Technology*, K. P. Johnston and J. M. L. Penninger, eds., *ACS Symp. Ser.*, **406**, 14 (1989).

Brennecke, J. F., D. L. Tomasko, and C. A. Eckert, "Naphthalene/Triethylamine Exciplex and Pyrene Excimer Formation in Supercritical Fluid Solutions," *J. Phys. Chem.*, **94**, 7692 (1990).

Brennecke, J. F., D. L. Tomasko, J. Peshkin, and C. A. Eckert, "Fluorescence Spectroscopy Studies in Dilute Supercritical Solutions," *Ind. Eng. Chem. Res.*, **29**, 1682 (1990).

Brennecke, J. F., and C. A. Eckert, "Molecular Interactions from Fluorescence Spectroscopy," *Proc. Int. Symp. on Supercrit. Fluids*, F. Perrut, ed., Nice, France, p. 263 (1988).

Bright, F. V., T. A. Betts, and J. Zagrobelny, "Kinetics and Mechanisms of Solute-Fluid and Solute-Solute Interactions in Supercritical Fluids: A Time-Resolved Fluorescence Study," *Proc. Int. Symp. on Supercrit. Fluids*, M. McHugh, ed., Boston, p. 49 (1991).

Brown, D., and J. H. R. Clarke, "A Comparison of Constant Energy, Constant Temperature and Constant Pressure Ensembles in Molecular Dynamics Simulations of Atomic Liquids," *Mol. Phys.*, **51**, 1243 (1984).

Capiomont, A., D. Bordeaux, and J. Lajzerowicz, "Structure Cristallographique de la Forme Quadrique du Nitroxyde Tétraméthyl-2,2,6,6, Pipéridineoxyle-1," *C. R. Acad. Sci.*, Paris, **275C**, 317 (1972).

Carlier, C., and T. W. Randolph, "Dense-Gas Solvent-Solute Clusters at Near-Infinite Dilution: EPR Spectroscopic Evidence," *AIChE J.*, **39** (May, 1993).

Chialvo, A. A., and P. G. Debenedetti, "On the Use of the Verlet Neighbor List in Molecular Dynamics," *Comput. Phys. Commun.*, **60**, 215 (1990).

Chialvo, A. A., and P. G. Debenedetti, "On the Performance of an Automated Verlet Neighbor List Algorithm for Large Systems on a Vector Processor," *Comput. Phys. Commun.*, **64**, 15 (1991).

Cochran, H. D., and L. L. Lee, "Solvation Structure in Supercritical Fluid Mixtures Based on Molecular Distribution Functions," *Supercritical Fluid Science and Technology*, K. P. Johnston and J. M. L. Penninger, eds., *ACS Symp. Ser.*, **406**, 27 (1989).

Cochran, H. D., and L. L. Lee, "Structure and Properties of Supercritical Fluid Mixtures from Kirkwood-Buff Fluctuation Theory and Integral Equation Methods," *Fluctuation Theory of Mixtures*, E. Matteoli and G. A. Mansoori, eds., Taylor and Francis, New York, p. 69 (1990).

Cochran, H. D., L. L. Lee, and D. M. Pfund, "Study of Fluctuations in Supercritical Solutions by an Integral Equation Method," *Proc. Int. Symp. on Supercrit. Fluids*, F. Perrut, ed., p. 245, Nice, France (1988).

Combes, J. R., K. P. Johnston, K. E. O'Shea, and M. A. Fox, "The

Influence of Solvent-Solute and Solute-Solute Clustering on Chemical Reactions in Supercritical Fluids," *Supercritical Fluid Technology*, F. V. Bright and M. E. P. McNally, eds., *ACS Symp. Ser.*, **448**, 31 (1992).
Debenedetti, P. G., "Clustering in Dilute, Binary Supercritical Fluid Mixtures: A Fluctuation Analysis," *Chem. Eng. Sci.*, **42**, 2203 (1987).
Debenedetti, P. G., and A. A. Chialvo, "Solute-Solute Correlations in Infinitely Dilute Supercritical Mixtures," *J. Chem. Phys.*, **97**, 504 (1992).
Debenedetti, P. G., and R. S. Mohamed, "Attractive, Weakly Attractive and Repulsive Near-Critical Systems," *J. Chem. Phys.*, **90**, 4528 (1989).
DeSimone, J. M., Z. Guan, and C. S. Elsbernd, "Synthesis of Fluoropolymers in Supercritical Carbon Dioxide," *Sci.*, **257**, 945 (1992).
Hansen, J.-P., and I. R. McDonald, *Theory of Simple Liquids*, Academic Press, New York (1986).
Hill, T. L., *Introduction to Statistical Thermodynamics*, Addison-Wesley, Reading, MA (1960).
Hirschfelder, J. O., C. F. Curtiss, and R. B. Bird, *Molecular Theory of Gases and Liquids*, Wiley, New York (1954).
Ikushima, Y., N. Saito, and M. Arai, "Supercritical Carbon Dioxide as Reaction Medium: Examination of Solvent Effects in the Near-Critical Region," *J. Phys. Chem.* **96**, 2293 (1992).
Johnson, J. K., J. A. Zollweg, and K. E. Gubbins, "The Lennard-Jones Equation of State Revisited," *Mol. Phys.*, **78**, 591(1993).
Johnston, K. P., S. Kim, and J. Combes, "Spectroscopic Determination of Solvent Strength and Structure in Supercritical Fluid Mixtures: A Review," *Supercritical Fluid Science and Technology*, K. P. Johnston and J. M. L. Penninger, eds., *ACS Symp. Ser.*, **406**, 52 (1989).
Johnston, K. P., and C. Haynes, "Extreme Solvent Effects on Reaction Rate Constants at Supercritical Fluid Conditions," *AIChE J.*, **33**, 2017 (1987).
Jorgensen, W. L., J. D. Madura, and C. J. Swenson, "Optimized Intermolecular Potential Functions for Liquid Hydrocarbons," *J. Amer. Chem. Soc.*, **106**, 6638 (1984).
Jorgensen, W. L., "Optimized Intermolecular Potential Functions for Liquid Alcohols," *J. Phys. Chem.*, **90**, 1276 (1986).
Jorgensen, W. L., and J. Tirado-Rives, "The OPLS Potential Functions for Proteins. Energy Minimizations for Crystals of Cyclic Peptides and Crambin," *J. Amer. Chem. Soc.*, **110**, 1657 (1988).
Jorgensen, W. L., J. M. Briggs, and M. L. Contreras, "Relative Partition Coefficients for Organic Solutes from Fluid Simulations," *J. Phys. Chem.*, **94**, 1683 (1990).
Kajimoto, O., M. Futakami, T. Kobayashi, and K. Yamasaki, "Charge-Transfer-State Formation in Supercritical Fluid: (*N*,*N*-Dimethylamino)benzonitrile in CF_3H," *J. Phys. Chem.*, **92**, 1347 (1988).
Kim, S., and K. P. Johnston, "Molecular Interactions in Dilute Supercritical Fluid Solutions," *Ind. Eng. Chem. Res.*, **26**, 1206 (1987).
Knauer, B. R., and J. J. Napier, "The Nitrogen Hyperfine Splitting Constant of the Nitroxide Functional Group as a Solvent Polarity Parameter: the Relative Importance for a Solvent Polarity Parameter of Its Being a Cybotactic Probe vs. Its Being a Model Process," *J. Amer. Chem. Soc.*, **98**, 4395 (1976).
Knutson, B. L., D. L. Tomasko, C. A. Eckert, P. G. Debenedetti, and A. A. Chialvo, "Local Density Augmentation in Supercritical Solutions: a Comparison Between Fluorescence Spectroscopy and Molecular Dynamics Results," *Supercritical Fluid Technology*, F. V. Bright and M. E. P. McNally, eds., *ACS Symp. Ser.*, **448**, 60 (1992).
Lajzerowicz-Bonneteau, J., "Molecular Structures of Nitroxides," *Spin Labeling: Theory and Applications*, L. J. Berliner, ed., p. 239, Academic Press, New York (1976).
Lee, L. L., *Molecular Thermodynamics of Nonideal Fluids*, Butterworths, Stoneham, MA, p. 247 (1988).
McGuigan, D. B., and P. A. Monson, "Analysis of Infinite Dilution Partial Molar Volumes Using a Distribution Function Theory," *Fluid Phase Equilibria*, **57**, 227 (1990).
McRae, E. G., "Theory of Solvent Effects on Molecular Electronic Spectra: Frequency Shifts," *J. Phys. Chem.*, **61**, 562 (1956).
Metropolis, N., A. W. Rosenbluth, M. N. Rosenbluth, A. H. Teller, and E. Teller, "Equation of State Calculations by Fast Computing Machines," *J. Chem. Phys.*, **21**, 1087 (1953).
Nicolas, J. J., K. E. Gubbins, W. B. Streett, and D. J. Tildesley, "Equation of State for the Lennard-Jones Fluid," *Mol. Phys.*, **37**, 1429 (1979).
Odian, G., *Principles of Polymerization*, Chap. 3, Wiley, New York (1981).
Peck, D. G., A. J. Mehta, and K. P. Johnston, "Pressure Tuning of Chemical Reaction Equilibria in Supercritical Fluids," *J. Phys. Chem.*, **93**, 4297 (1989).
Petsche, I. B., and P. G. Debenedetti, "Influence of Solute-Solvent Asymmetry Upon the Behavior of Dilute Supercritical Mixtures," *J. Phys. Chem.*, **95**, 386 (1991).
Petsche, I. B., and P. G. Debenedetti, "Solute-Solvent Interactions in Infinitely Dilute Supercritical Mixtures: A Molecular Dynamics Investigation," *J. Chem. Phys.*, **91**, 7075 (1989).
Prausnitz, J. M., *Molecular Thermodynamics of Fluid Phase Equilibria*, Prentice-Hall, Englewood Cliffs, NJ, p. 107 (1969).
Randolph, T. W., and C. Carlier, "Free Radical Reactions in Supercritical Ethane: A Probe of Supercritical Fluid Structure," *J. Phys. Chem.*, **96**, 5146 (1992).
Randolph, T. W., D. S. Clark, H. W. Blanch, and J. M. Prausnitz, "Enzymatic Oxidation of Cholesterol Aggregates in Supercritical Carbon Dioxide," *Sci.*, **34**, 1354 (1988).
Reid, R. C., J. M. Prausnitz, and T. K. Sherwood, *The Properties of Gases and Liquids*, McGraw Hill, New York, pp. 17, 548 (1977).
Schneider, D. J., and J. H. Freed, "Calculating Slow Motional Magnetic Resonance Spectra," *Biological Magnetic Resonance*, Vol. 8, L. J. Berliner and J. Reubens, eds., Plenum Press, New York (1989).
Smit, B., P. De Smedt, and D. Frenkel, "Computer Simulations in the Gibbs Ensemble," *Mol. Phys.*, **68**, 931 (1989).
Verlet, L., "Computer 'Experiments' on Classical Fluids: I. Thermodynamical Properties of Lennard-Jones Molecules," *Phys. Rev.*, **159**, 98 (1967).
Wu, R.-S., L. L. Lee, and H. D. Cochran, "Structure of Dilute Supercritical Solutions: Clustering of Solvent and Solute Molecules and the Thermodynamic Effects," *Ind. Eng. Chem. Res.*, **29**, 977 (1990).
Yonker, C. R., and R. D. Smith, "Solvatochromism: A Dielectric Continuum Model Applied to Supercritical Fluids," *J. Phys. Chem.*, **92**, 235 (1988).

Appendix I: Simulation Details

Molecular dynamics

All of the production simulation runs described here were NVT molecular dynamics simulations (Allen and Tildesley, 1986) of 1 solute molecule in 599 solvent molecules. The simulations were carried out by the constraint method, with leap-frog integration (Allen and Tildesley, 1986). A few NVE runs were also carried out for checking purposes; in these runs, the equations of motion were integrated using the velocity form of the Verlet algorithm. The length of the cubic simulation box was determined by the density under consideration in a given run. Both solute and solvent were assumed to be Lennard-Jones molecules, with parameters generated as described above and reported in Table 1. The intermolecular potential was cut off at long range, with the minimum cutoff at $2.8\sigma_{12}$. At the lower densities for which results are reported, the cutoff was even longer in order to capture faithfully the more gas-like regime, where the particles could be separated by distances on the order of the cutoff distance; the cutoff in this case was taken as twice the average expected molecular separation. A run consisted of 2×10^5 MD time steps, each of duration 0.003 in units of $\sigma_1\sqrt{m_1/\epsilon_1}$, where 1 is the solvent species. Assuming that the solvent is ethane, based on its molecular mass and Table 1, the time step corresponds to 6.751×10^{-15} s, which translates to a total simulated time of 1.35×10^{-9} s. This is an extremely long simulated time compared to typical liquid simulations (Allen and Tildesley, 1986).

The starting configuration was a simple cubic lattice of mol-

ecules having Gaussian distributed velocities corresponding to the chosen temperature. The system was allowed to equilibrate for 4,000 time steps, the first 2,000 of which were at three times the nominal temperature to speed the melting of the initial defective crystal; the temperature was reset after 2,000 steps by rescaling the molecular momentums. To speed up the simulations, the Verlet neighbor list (Allen and Tildesley, 1986) technique was implemented, in association with the automatic list updating method described by Chialvo and Debenedetti (1990, 1991). As recommended by Chialvo and Debenedetti, the SKIN parameter was taken to be 0.5.

Implementation

Several computer programs were written to carry out these simulations. All were run on a Hewlett-Packard 9000/720 Unix workstation. The production MD simulations were written in Pascal, and their output checked against an independently written, but unoptimized, FORTRAN MD code, as well as a simple Monte Carlo code. A typical NVT-MD run with 600 molecules and 2×10^5 time steps consumes some 16 hours of CPU time. For some of the comparison runs, much shorter simulations were adequate. The comparison with the results of Brown and Clarke (1984), for example, required a run of only about 15 min.

Several modifications to the usual analysis techniques were adopted to increase the speed and reduce the disk storage requirements of the simulations.

Radial Distribution Functions. The usual way of computing the radial distribution functions, $g_{ij}(r)$, is to store the configurations of the molecules periodically on disk and, once the simulation has finished, to read them and compute the necessary separation histograms (Allen and Tildesley, 1986). For a system of 600 molecules and runs of several hundred thousand time steps, this would be prohibitive in terms of disk space, requiring tens to hundreds of megabytes in order to store every configuration. The usual approach is to analyze only some fraction of the configurations. Instead, the radial distribution functions were computed in place using *every* configuration, by storing in memory the pair separation arrays for each type of pair (1-1 or 1-2). Of course, this restricts the most precise computation of $g_{ij}(r)$ to within the separations that are updated on each time step; however, the longer-ranged $g_{ij}(r)$ may be computed during Verlet neighbor list updates, when all intermolecular separations become available. For the conditions we studied and the SKIN parameter used, this frequency varied between every 10 and every 40 MD steps.

The memory requirements for this approach are much greater than for a traditional MD simulation. (A little less than 2Mb of memory is needed to store the pair arrays and the neighbor list for 600 particles.) Memory, however, is typically cheap and plentiful on modern workstations, whereas disk storage space is often still not as abundant as on larger supercomputers. We anticipate that this trend in scientific computing will continue as workstations become cheaper and more numerous; programming techniques for conserving memory in scientific computations will become less relevant relative to those for conserving disk space.

Diffusion Coefficients. The diffusion coefficients for both component 1 (D^*_{11}) and for component 2 in component 1 (D^*_{12}) were computed by integrating the velocity autocorrelation function of the molecules. The autocorrelation function was also computed in place by storing in a circular buffer a velocity history of 2,500 time steps or channels. Every 10 time steps, the buffer velocities were correlated against themselves (see, for example, Allen and Tildesley, 1986) and added into an accumulator array. For the solvent, the autocorrelation function was averaged over 10 molecules; in the case of the solute, since there was only one molecule, statistics were collected only for this molecule and may be expected to be somewhat poorer.

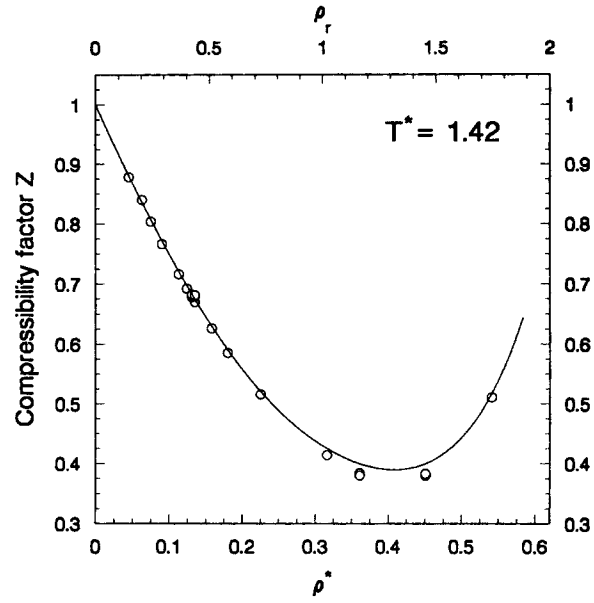

Figure A1. Compressibility factor, $z \equiv P/\rho kT$, against reduced density, ρ^*, on the isotherm $T^* = 1.42$.

The points are simulation results, and the line is the equation of state of Johnson et al. (1992).

Appendix II: Simulation Verification

Since we are using the simulation results to draw far-reaching conclusions in this article it is obviously incumbent upon us to check the results to the best of our ability. We carried out tests of several types to verify the correct operation of the simulation program.

Low density limit

In the limit of low density, a radial distribution function should degenerate into the Boltzmann factor of the intermolecular potential energy function, since the only interactions present are direct pair interactions:

$$\lim_{\rho\to 0} g_{ij}(r) = \exp[-\beta\Gamma_{ij}(r)] \qquad \text{(A1)}$$

We carried out simulations at a reduced density $\rho^* = 0.063$, and the simulated results agreed well with Eq. A1.

Pseudomixture

To test the algorithms for computing each of the $g_{ij}(r)$, we carried out simulations of mixtures with *identical molecular parameters*: these were not really mixtures at all. Under these

Table A1. Comparison with Simulations of Brown and Clarke (1984)

	B&C [NVE]	B&C [NVT]	This Work [NVT]
U_c/NkT	−8.331	−8.315	−8.320
E/NkT	−6.836	−6.774	−6.828
D^*_{11} [vacf]	0.0341	0.0334	0.0336
D^*_{11} [disp]	0.0328	0.0327	0.0334

conditions, all of the $g_{ij}(r)$ should be equal. This was verified to be the case, although the statistics are obviously not as good for the low-concentration pseudocomponent, since there are fewer pairs to count in the histograms.

Lennard-Jones equation of state

The substantial amount of existing L-J simulation data has been synopsized by Nicolas et al. (1979) by fitting it to the modified Benedict Webb Rubin equation of state. This synopsis has recently been updated (Johnson et al., 1992). In Figure A1 we plot compressibility factor z against density ρ^* along the $T^* = 1.42$ isotherm, which is the one we have been simulating throughout the article. The points are the simulation results, while the line is computed from the L-J equation of state of Johnson et al. (1993). The excellent comparison between the two proves that our results are the same as those measured in previous simulations. The initial slope of the curve agrees with the second virial coefficient, as computed for L-J molecules by Hirschfelder et al. (1954). The agreement between the equation of state for pure solvent and our results, which are for solute at infinite dilution in solvent at the same bulk conditions, supports our assertion that there is no global effect on the solvent thermodynamics due to the solvent-solute clustering.

Typical simulation results

We have tested our program using several sets of parameters previously reported in the literature. We compared $g(r)$ for a pure L-J fluid ($T^* = 1.273$, $\rho^* = 0.85$) computed using both our NVT-MD and NVT-MC codes to the results of Verlet as reported by Lee (1988). The agreement is excellent in both cases, and the plotted curves are indistinguishable.

For a more comprehensive thermodynamic test, we have simulated the system discussed by Brown and Clarke (1984).

This is a 256-particle system of L-J molecules near the L-J triple point, which they simulated using several techniques, among them the constraint method for NVT-MD. Table A1 shows the comparison of the latter to our run for the same conditions, time step and number of steps. We compare configurational internal energy U_c/NkT, total internal energy E/NkT, and diffusion coefficient, D^*_{11} (computed via two different methods), all of which agree within the experimental accuracy of the simulations. In the table, [vacf] denotes a diffusion coefficient calculated by integrating the velocity autocorrelation function, while [disp] denotes one calculated from the slope of (displacement) against time.

Finally, we have duplicated one run from the study by Petsche and Debenedetti (1989) for an attractive mixture of 863 solvents and 1 solute at $\rho^* = 0.35$ and $T^* = 1.4$. We obtained the same $g_{ij}(r)$ as the latter authors to within a couple of percent.

Time step and system size

We checked the adequacy of the time step $\Delta t^* = 0.003$ by carrying out simulations at $\rho^* = 0.135$ with time steps of $0.5\Delta t^*$ and $2\Delta t^*$, respectively. In each case, the total number of time steps was adjusted to obtain the same simulated time. The results were not distinguishable within the experimental error. Therefore, the chosen Δt^* is verified to be adequate. As a further check, we simulated a systems of 1,000 and 1,800 molecules, again at $\rho^* = 0.135$ and using $\Delta t^* = 0.003$. The results were indistinguishable from those obtained using 600 molecules.

Diffusion coefficient scaling

Using the theory of Chapman and Enskog for diffusion coefficients in terms of collision integrals, as outlined by Reid et al. (1977), we computed the ratio D^*_{11}/D^*_{12} using the parameters and thermodynamic conditions appropriate to our system. This ratio ought to be independent of density, at least in the low-density regime where this approach is valid. The Chapman-Enskog value was computed to be 2.7, which we also observed in the simulations (see Figure 6a).

Potential cutoff

We investigated the effects of the cutoff imposed in the L-J potential function by simulating several state point with different cutoffs. No differences were observed in the thermodynamic functions, once the appropriate tail corrections were added; in fact, there are points on the z vs. ρ^* curve of Figure A1 which were computed using several different cutoff values. As described above, we set our cutoff to be at least $3.695\sigma_{11}$ ($= 2.8\sigma_{12}$ for the parameters in our simulations). This is greater, for example, than the value of approximately $2.5\sigma_{12}$ used by Knutson et al. (1992). Further, at low density we increased the cutoff in proportion to the average particle separation.

Manuscript received Sept. 21, 1992, and revision received Nov. 19, 1992.